# Recurrence-Based Characterization of Stickiness in Hamiltonian Systems


**R. L. Viana, L. C. Souza, M. R. Sales, M. Mugnaine, J. D. Szezech Jr., I. L. Caldas, N. Marwan, and J. Kurths**

**Abstract** In quasi-integrable Hamiltonian systems, certain chaotic orbits become trapped around periodic islands for extended periods before escaping to the chaotic sea, a phenomenon known as stickiness. In fusion plasmas, the stickiness effect manifests in the prolonged trapping of magnetic field lines in a specific region for many toroidal turns, influencing plasma transport. We apply here a novel concept based on recurrence plots, revealing the existence of a hierarchical structure of islands around islands where chaotic orbits become trapped. This analysis is conducted for a Hamiltonian system describing the magnetic field lines in a Tokamak. Furthermore, utilizing this quantifier, we can distinguish between different levels of this structure and compute the cumulative distribution of trapping times.

## 1 Introduction

The phase space of quasi-integrable Hamiltonian systems often exhibits distinctive behaviors, characterized by the presence of regular and chaotic regions. Between these domains lies a transition layer, where regular and irregular motion can either

R. L. Viana (✉)
Department of Physics, Federal University of Paraná, Curitiba, Brazil
e-mail: viana@fisica.ufpr.br

L. C. Souza
Departamento de Física, Universidade Federal do Paraná, Curitiba, Paraná, Brazil

L. C. Souza · M. Mugnaine · I. L. Caldas
Instituto de Física, Universidade de São Paulo, São Paulo, São Paulo, Brazil

M. R. Sales
Departamento de Física, Universidade Estadual Paulista (UNESP), Rio Claro, São Paulo, Brazil

J. D. Szezech Jr.
Programa de Pós-Graduação em Ciências, Universidade Estadual de Ponta Grossa, Ponta Grossa, Paraná, Brazil

N. Marwan · J. Kurths
Potsdam Institute for Climate Change, Potsdam, Germany



Y. Hirata et al. (eds.), *Recurrence Plots and Their Quantifications: Methodological Breakthroughs and Interdisciplinary Discoveries*, Springer Proceedings in Complexity,
https://doi.org/10.1007/978-3-031-91062-3_6

coexist or remain separate. This behavior depends on both the number of degrees of freedom in the system and the properties of the limiting surface. In the regular dynamics, orbits follow periodic and quasiperiodic trajectories on invariant tori, while chaotic orbits densely fill regions of the energy surface in phase space [1].

The intricate interplay of regular and chaotic orbits gives rise to unusual statistical properties for trajectories within the chaotic component of the phase space [2]. Additionally, this complex behavior leads to phenomena such as anomalous diffusion [3] and dynamic traps [4]. Plasma physics is a field where chaotic behavior plays a crucial role, particularly in the study of magnetic confinement plasmas [5]. Chaotic motion is prevalent in toroidal plasma devices like Tokamaks, where time-dependent perturbations lead to anomalous transport phenomena [6]. Therefore, comprehending the physical factors influencing chaotic transport is essential for the development of effective magnetic confinement devices.

The mixed phase space leads to the formation of dynamical traps in the form of perforated tori, called cantori, near periodic islands, acting as intermittent transport barriers and forming sticky regions. The duration of orbit confinement within these sticky regions depends on the size of holes in the tori [7]. However, such trapping influences the long-term calculation of dynamical quantifiers, such as Lyapunov exponents. Therefore, a quantitative characterization of sticky behavior is crucial to comprehend its impact on time averages of dynamical quantities. Initial conditions in the chaotic region may experience different dynamical behavior, making it useful to consider a finite-time analysis of the evolution of these initial conditions to describe chaotic evolution accurately.

In phase spaces with sticky regions, the Lyapunov exponent is not an optimal choice to detect chaotic orbits due to trapping around the islands, that causes its values to approach zero. Other methods, such as weighted Birkhoff averages [8], the 0-1 test [9], SALI and GALI [10], etc., have been proposed to circumvent this problem. However, these methods often require long time series for reliable accuracy. In cases where only a short time series is available, recurrence quantification analysis (RQA) [11–14] is preferred.

In this work, we employ a RQA based on an intrinsic property of the dynamical system: Slater's theorem [15, 16], which states that quasiperiodic orbits lying on invariant circles can have at most three different return times. By defining a region of recurrence and counting the time it takes for the orbit to return to this region, we obtain recurrence times and are able to construct the recurrence plots. Recurrence plots (RP) are used to find the recurrence in a time series. They also are used to estimate recurrence times, with white vertical lines in the RP serving as a lower estimate of recurrence time [17–19].

In the pursuit of controlled thermonuclear fusion, the Hamiltonian description is employed to study magnetic field lines in Tokamaks [20]. In the context of a symmetric magnetohydrodynamical equilibrium, the magnetic field lines are governed by the Hamiltonian canonical equations, where the ignorable coordinate takes the role of time. This treatment allows the complex dynamics of the magnetic field lines to be effectively described using symplectic two-dimensional nonlinear maps. The main objective of the present work is to develop and apply methods to clearly differentiate between sticky and non-sticky orbits. We shall accomplish this task by using

recurrence-based quantifies, which provide robust tools for analyzing the temporal patterns and spatial quantities within the phase space and allow us to obtain a deeper insight of the underlying mechanism of stickiness in Hamiltonian systems.

We used RPs to characterize the dynamics of a nonlinear system, applying RQA to identify regular, chaotic, and sticky regions in a magnetic field lines model called Tokamap [21]. The stickiness effect changes the escape times of trajectories, impacting the effective transport fluxes [22]. The RQA indicator we choose is based on the Shannon entropy of recurrence times, known as the recurrence time entropy (RTE) [23, 25], originally proposed without any connection to RPs.

This paper is organized as follows: in Sect. 2 the area-preserving two-dimensional map proposed to investigate the magnetic field line structure is presented. In Sect. 3 the quantifier based on recurrence time is introduced. In Sect. 4 we discuss the application of the recurrence time entropy to the study of stickiness in the Tokamap. Finally, in the last Section, we report our conclusions.

## 2 Magnetic Field Line Map

Tokamaks are toroidal devices for magnetic confinement of fusion plasmas. They are considered as promising candidates for maintaining thermonuclear fusion with the goal of energy production. This hope is the chief stimulus behind the ITER (International Thermonuclear Energy Reactor) project, an international collaboration involving 35 countries whose goal is to build the largest Tokamak in the world, with an estimated $\sim$500 MW of fusion power. ITER, currently being assembled in the southern France, is the most expensive science experiment ever, and is expected to start its operation in 2034.

In spite of its inherent complexity and huge size, the physical principles underlying the Tokamak concept are relatively simple. A toroidal plasma is confined using two magnetic fields: a toroidal field $\mathbf{B}_T$ generated by external coils, and the poloidal field $\mathbf{B}_P$, created by the plasma current. The resulting field $\mathbf{B} = \mathbf{B}_T + \mathbf{B}_P$ has helical magnetic lines of force lying on nested tori called magnetic surfaces. Under fairly general symmetry conditions, we can define a flux function $\psi$ which has a constant value on a magnetic surface: $\mathbf{B} \cdot \nabla\psi = 0$.

The coordinates used to locate magnetic field lines in a Tokamak are illustrated in Fig. 1a. The magnetic axis is a degenerate magnetic surface, and $R_0$ is the distance between the magnetic axis and a vertical axis. The toroidal angle $\zeta$ is measured along the long way around the torus, whereas the (normalized by $2\pi$) poloidal angle $\theta$ goes along the short way. If we consider a fixed plane at $\zeta = 0$, the field line position therein is described by coordinates $(r, \theta)$ with its center on the magnetic axis Fig. 1b. The flux function $\psi$ is the remaining coordinate, such that the plasma edge is located at $\psi = 1$, whereas $\psi = 0$ is the magnetic axis position.

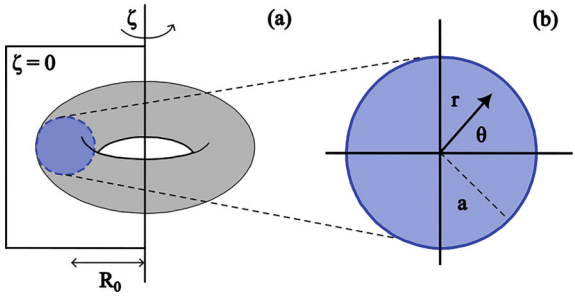


**Fig. 1** **a** Coordinate system for magnetic field lines in a Tokamak; **b** a cross section at $\zeta = 0$ plane

Using the coordinates $(\psi, \theta, \zeta)$, the magnetic field line equations can be expressed in a form which resembles Hamilton's equation

$$\frac{d\psi}{d\zeta} = -\frac{\partial H}{\partial \theta}, \tag{1}$$

$$\frac{d\theta}{d\zeta} = \frac{\partial H}{\partial \psi}, \tag{2}$$

where $(\psi, \theta)$ are the canonical variables, $\zeta$ plays the role of time, and $H$ is the field line Hamiltonian. In a symmetrical configuration the latter does not depend on the "time" $\zeta$, and the one-degree-of-freedom system is thus integrable.

Moreover, $H$ depends only on $\psi$, such that $(\psi, \theta)$ are action-angle variables, and the Hamilton's equations read

$$\frac{d\psi}{d\zeta} = 0, \tag{3}$$

$$\frac{d\theta}{d\zeta} = \frac{dH}{d\psi} \equiv \frac{1}{q(\psi)}, \tag{4}$$

with the so-called safety factor as

$$q(r) = \frac{r B_0}{R_0 B_\theta(r)}, \tag{5}$$

where $B_0$ is the toroidal field at magnetic axis, and $B_\theta(r)$ is the poloidal field as a function of radius $r$. The magnetic surfaces in this approximation are coaxial cylinders with $\psi = (r/a)^2$. A safety factor radial profile consistent with Tokamak magnetic field and Ohmic discharge is [26]

$$q(\psi) = \frac{4q_0}{(2-\psi)(2-2\psi+\psi^2)}, \tag{6}$$

where $q_0 = q(\psi = 0) = 1$. We also choose $q(\psi = 1) = 4$ at plasma edge.

In a Tokamak, the presence of instabilities or external magnetic fields causes perturbations in the magnetic field lines, breaking their symmetry and allowing chaotic motion. These perturbations can be described by a non-integrable Hamiltonian, and if the perturbation is small, the Hamiltonian can be approximated as a quasi-integrable system,

$$H(\psi, \theta, \zeta) = \int_0^{\psi} \frac{d\psi'}{q(\psi')} + \varepsilon H_1(\psi, \theta, \zeta), \tag{7}$$

where $\varepsilon$ is the perturbation amplitude. Integrating the canonical equations (1)–(2) for the Hamiltonian (7) gives the magnetic field lines in the non-symmetric system. The numerical integration the equations can be very costly for long times, however, a considerable simplification arises from using a Poincaré section. This can be obtained by sampling the coordinates $(\psi_n, \theta_n)$ of the $n$th intersection of a given magnetic field line with the $\zeta = 0$ plane. It results in a two-dimensional mapping with discrete time $n$. The magnetic Gauss law $\nabla \cdot \mathbf{B} = 0$ implies that the magnetic flux must be conserved, meaning that the mapping must be area-preserving. Moreover, $\psi = (r/a)^2$ implies that $\psi \geq 0$ for all $n$.

A paradigmatic field line map was proposed by Balescu and coworkers, the *Tokamap* [21], which satisfies all the conditions listed above. The equations of motion are given by,

$$\psi_{n+1} = \frac{1}{2}\left\{ P(\psi_n, \theta_n) + \sqrt{[P(\psi_n, \theta_n)]^2 + 4\psi_n}, \right\}, \tag{8}$$

$$P(\psi_n, \theta_n) = \psi_n - 1 - \frac{k}{2\pi}\sin(2\pi\theta_n), \tag{9}$$

$$\theta_{n+1} = \theta_n + \frac{1}{q(\psi_n)} - \frac{k}{4\pi^2}\frac{1}{(1+\psi_{n+1})^2}\cos(2\pi\theta_n) \qquad (\text{mod } 1) \tag{10}$$

$$q(\psi) = \frac{4}{(2-\psi)(2-2\psi+\psi^2)}, \tag{11}$$

where $k$ is a variable parameter representing the strength of the non-symmetrical perturbation acting on the Tokamak. In a real setting, this perturbation is created by a magnetic field generated by helical windings, so $k$ can be considered proportional to the current flowing through the windings [27]. The tokamap adheres to physical requirements, while the perturbation is simplified by using only a sinusoidal term. More general perturbations can be viewed as expansions in trigonometric functions, making the tokamap a simple, yet representative model of more complex scenarios found in physical applications.

Iterating the map (8)–(10), we have in the case of no perturbation ($k = 0$), $P(\psi_n) = \psi_n - 1$ and the Tokamap reduces to a simple twist map, which describes an integrable system, as shown in Fig. 2a. When $k$ is small, the phase space is composed of invariant curves with some degree of distortion and also some periodic island chains, Fig. 2b. As the perturbation increases, the chaotic region surrounding the islands chains expands, Fig. 2c. A subsequent further increase in the perturbation

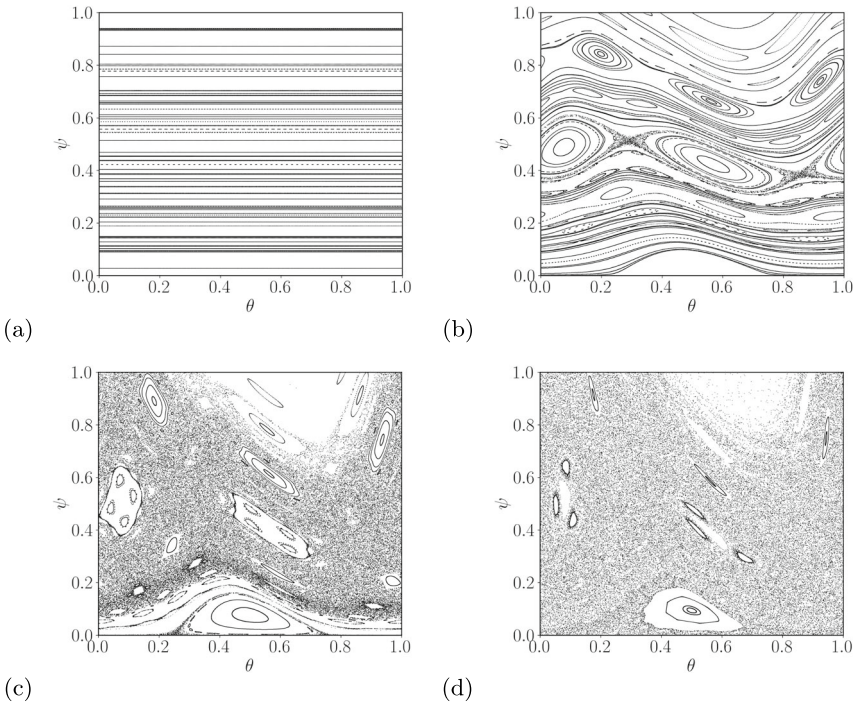


**Fig. 2** Phase space of the Tokamap with 1500 map iterations for $k = 0.0$ in (**a**), $k = 3.0$ in (**b**), $k = 5.0$ in (**c**) and $k = 2\pi$ in (**d**)

causes the chaotic region to span the entire phase space, yet certain periodic islands persist within the chaotic sea, Fig. 2d.

Some chaotic orbits spend a considerable amount of time around periodic islands, exhibiting the stickiness effect, as we can observe around the islands of period three in Fig. 2d. Although a sticky orbit is also chaotic and area-filling, it occupies a slimmer region of the phase space.

## 3 Recurrence Time Entropy

Given a time series corresponding to a map orbit $\mathbf{x}_i = (\psi_i, \theta_j)^\intercal$ $(i = 1, 2, \ldots, N)$, the corresponding recurrence matrix elements are defined as

$$R_{ij} = \Theta(\varepsilon - \|\mathbf{x}_i - \mathbf{x}_j\|), \tag{12}$$

where $N$ is the length of the time series, $\varepsilon$ is the threshold parameter, $\Theta$ is the Heaviside function, and $\|\mathbf{x}_i - \mathbf{x}_j\|$ is the spatial distance between two states at at

different times $i$ and $j$, here calculated with the supremum (or maximum) norm. The Euclidean norm could also be used, yielding similar results [13]. However, considering a fixed threshold $\varepsilon$, the maximum norm is computationally faster than the Euclidean norm. Recurrence plots (RP) are graphical representations of this recurrence matrix [28].

The matrix $R$ is symmetric and binary, whose elements are equal to 1 when the two states are recurrent and 0 otherwise. If the threshold $\varepsilon$ is too large, we would record too many recurrences, resulting in a barely distinguishable RP. On the other hand, for a too small $\varepsilon$, recurrences would be rarely observed. A good compromise is to consider $\varepsilon$ to be 10% of the time series standard deviation $\sigma$ [13, 29], a more systematic study on this selection can be found in [30].

The recurrent states are represented by colored dots in the RP, and display various diagonal structures. In Fig. 3a the phase space for three initial conditions is shown with the corresponding recurrence matrix for the first 1000 iterations of (b) a quasiperiodic orbit, (c) a chaotic orbit, and (d) a sticky orbit of the Tokamap (8)–(10) with $k = 3\pi/2$. The RP of a quasiperiodic orbit is composed of uninterrupted diagonal lines. The vertical distances between these lines display a regularity and

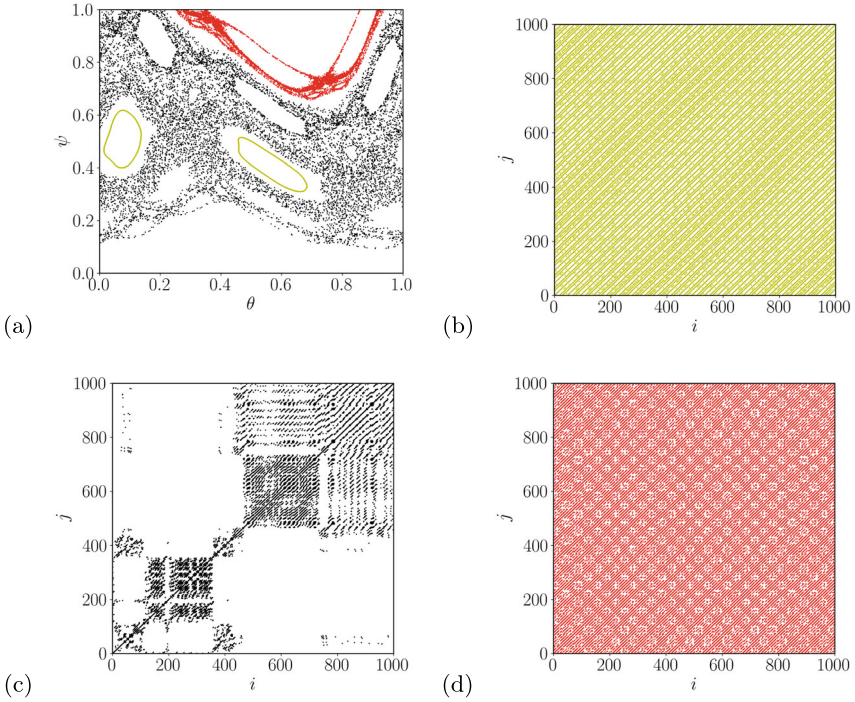


**Fig. 3** **a** Phase space with a quasiperiodic orbit (yellow), a chaotic orbit (black), and a sticky orbit (red) of the Tokamap with $k = \frac{3\pi}{2}$. Recurrence matrix of the **b** quasiperiodic orbit, **c** the chaotic orbit, and **d** the sticky orbit for the first 1000 iterates of the map

correspond to the different return times of the orbit [17–19]. The RP of a chaotic orbit displays short diagonal lines, and the vertical distances between them are not as regular as in the quasiperiodic case. In the RP of a sticky orbit, the diagonal lines present some level of regularity, with intermediary size of these lines.

Numerous dynamical quantifiers rely on RP structures, based on diagonal line lengths ($l$) and vertical line lengths ($\nu$), such as determinism, laminarity, recurrence rate, and various others, constituting a rich array of tools derived from RPs for dynamical analysis [11]. There are also, quantifiers based on the Shannon entropy of the diagonal line lengths [31],

$$S = -\sum_{l=l_{min}}^{l_{max}} p(l) \ln p(l), \tag{13}$$

where $l_{max}$ ($l_{min}$) is the length of the longest (shortest) diagonal line, in this work, we consider $l_{min} = 1$, $p(l) = P(l)/N_l$ and $P(l)$ are the relative distribution and the total number of line segments with length $l$, respectively, and $N_l$ is the total number of line segments, $P(l)$ is the frequency distribution (or histogram). Given that the vertical distance between the lines is an estimate of the recurrence times of an orbit, we consider the Shannon entropy using the "white" vertical lines of the RP in (13) [17, 23]. The total number of white vertical lines (recurrence times) of length $\nu$ is given by

$$p_w(\nu) = \sum_{i,j=1}^{N} R_{ij} R_{ij+\nu} \prod_{k=0}^{\nu-1} (1 - R_{ij+k}). \tag{14}$$

An emerging idea suggests using the recurrence time distribution derived from recurrence plots for identifying regions associated with stickiness, as proposed in [23, 32]. For this purpose, we define the Recurrence Time Entropy RTE,

$$\mathrm{RTE} = -\sum_{\nu=\nu_{min}}^{\nu_{max}} p_w(\nu) \ln p_w(\nu). \tag{15}$$

The RTE is able to characterize the dynamics as a consequence of Slater's theorem, that states that for any irrational linear rotation, with rotation number $\omega$ over a unit circle, there are at most three different return times to a connected interval of size $\delta < 1$. By counting the number of return times (or recurrence times) or in this case the white vertical lines, we can distinguish between the different kinds of solutions of a nonlinear system. If it is one, the orbit is periodic, what correspond to RTE $= 0$, and if it is equal to three, the orbit is quasiperiodic, resulting in a small RTE. If the number of return times is larger than three, then the orbit is chaotic, corresponding to a large RTE. The sticky orbit spends a long time in the neighborhood of an island in which it exhibits a motion similar to quasiperiodic dynamics. This was seen in the recurrence matrix, Fig. 3d. Thus, the RTE of sticky orbits is smaller than the chaotic ones, but higher than a quasiperiodic orbit.

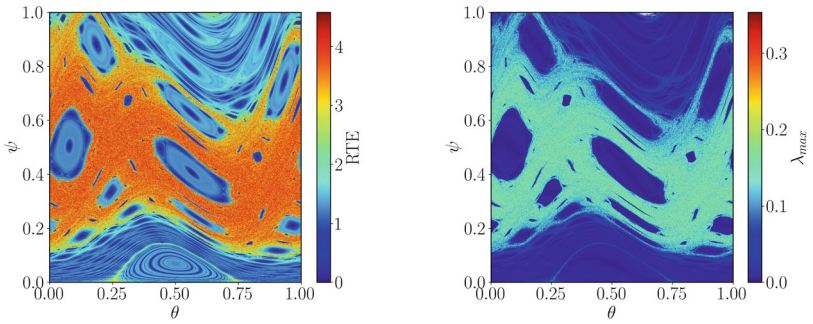


(a)

**Fig. 4** **a** Recurrence time entropy and **b** largest Lyapunov exponent, for the Tokamap with $k = 4.5$ iterated for $N = 10^3$ times

In Fig. 4, we show the RTE (a) and the largest Lyapunov exponent $\lambda_{max}$ (b) for an uniform distributed mesh of initial conditions of the Tokamap with $k = 4.5$. The Lyapunov exponent was computed using the method of Eckmann-Ruelle [33], where the Jacobian matrix is written as the product of an orthogonal matrix and an upper triangular matrix. The Jacobian becomes a triangular matrix itself, whose eigenvalues are its diagonal elements. Therefore, the Lyapunov exponents can be expressed in terms of these diagonal elements.

The RTE and the Lyapunov exponents are visually correlated [23, 24]. In the chaotic sea, $\lambda_{max}$ is large and so is the RTE. In the islands, $\lambda_{max}$ goes to zero and the RTE is low. Furthermore, in the neighbourhood of the islands the RTE takes on intermediary values, indicating that in these regions the orbits get trapped. In Hamiltonian systems the Lyapunov exponent has a slow convergence rate [1] and the trapping of chaotic orbits around quasiperiodic regions causes the Lyapunov exponent to be close to zero, resembling the quasiperiodic behaviour. Since the RTE clearly distinguishes between quasiperiodic and chaotic orbits, even considering small time series [32], it is a better quantifier of the dynamics.

## 4 Stickiness, Recurrence Time Entropy, and Trapping Time Distribution

It is possible to consider recurrence plots to characterize the stickiness effect [32, 34]. In this work, we apply one such characterization to the Tokamap, by considering the evolution of a single chaotic orbit using the parameter value $k = 3\pi/2$ for convenience (other values of $k$ would result in qualitatively similar results). For long times, a single chaotic orbit fills in a region of the phase space, approaching a large number of periodic islands and staying there for a long but finite time, before escaping to the chaotic region. Thus, it is better to consider a finite-time RTE with $n \ll N$ so

as to understand the transition between different dynamical regimes. We calculated the RTE for a single chaotic orbit in windows of size $n$, RTE$(i)(n)$ $i = 1, 2, \ldots, M$, where $M = N/n$, and define the probability distribution of the finite-time RTE, $P(\text{RTE}(n))$, by computing a frequency histogram of RTE$(i)(n)$ such as the one shown in Fig. 5a for $N = 10^{11}$ and $n = 200$. Given that the orbit visits different sticky regions with varying trapping times, we chose a very long orbit with $N = 10^{11}$ iterations. The choice of $n$ is arbitrary; choosing a large value could mix stickiness and the chaotic sea; on the other hand, taking a small value highlights local fluctuations. We found that $n = 200$ is a good compromise for describing the tokamap. The same methodology was employed to detect the stickiness region in an $\mathbf{E} \times \mathbf{B}$ model [35]. The changes in the RTE(200) values indicates changes of dynamical behaviour, which are the causes of the many modes observed in the corresponding probability distribution.

In Fig. 5b, we show the phase space position $(\psi, \theta)$ for the RTE(200) time series with different colours corresponding to different ranges of RTE(200). The colours match the distinct peaks depicted in Fig. 5a, such that each peak is related to a different

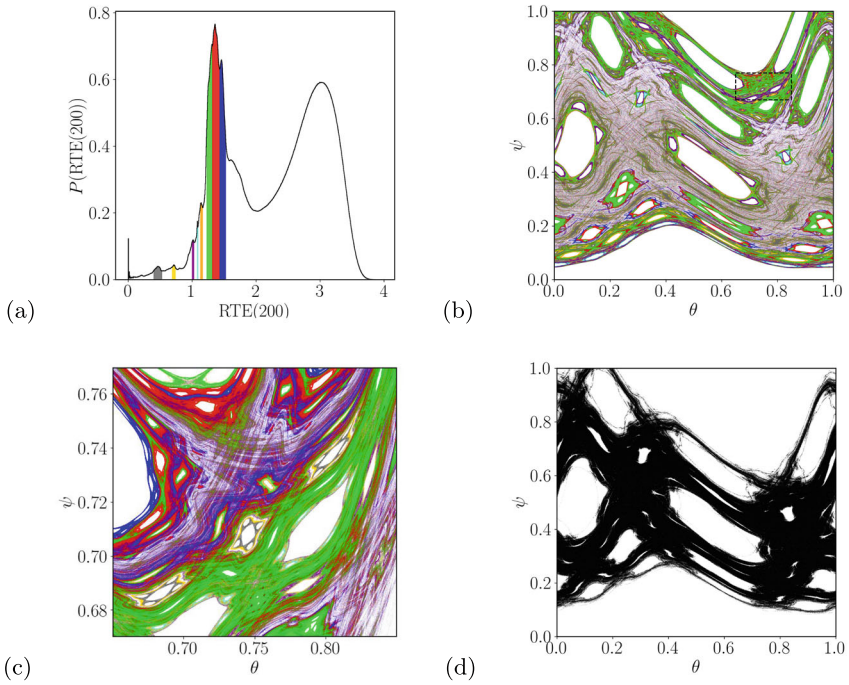


**Fig. 5** **a** Finite-time RTE distribution for a single chaotic orbit, with $n = 200$ $N = 10^{11}$, and $k = 3\pi/2$. **b** The phase space points that generate the small RTE(200) values peaks in (**a**). **c** is a magnification of the region indicated by the black dashed lines. **d** The phase space that generate the larger peak for high values of RTE in the distribution

region of trapping. The stickiness effect happens when the orbit gets trapped inside one of the levels of a hierarchical structure of island-around-islands. This structure correspond to the multi-modal distribution of RTE(200), where the largest maximum correspond to a high RTE value, so the orbit is in the chaotic sea. When the orbit is trapped near an island, the RTE is low and the distribution exhibits smaller peaks, for each level of this structure.

The recurrence time entropy RTE is able to distinguish among the different regions where the orbit gets trapped for some time, as well the fully chaotic region of the phase space. The red and yellow peaks correspond to regions that trace the stable and unstable manifolds in the region where the trapped particles leave the sticky region [cf. Fig. 5c]. In Fig. 5d are shown the phase space points corresponding to the largest peak in the distribution, i.e., the hyperbolic (non-sticky) part of the chaotic orbit.

Systems where the stickiness effect is present exhibit a bi-modal distribution of finite-time Lyapunov exponents (FTLE) [36], consisting of two peaks: one representing the chaotic component of the orbit and the other corresponding to the stickiness when the orbit is trapped. Harle and Feudel [37] suggested that the stickiness peak is actually composed of multiple peaks, each representing a different level of the hierarchical structure of islands-around-islands. The $RTE$ allows us to obtain this multi-modal distribution and differentiate the various levels of stickiness in the phase space. Moreover, it is possible to measure the time spent in each sticky region, i.e. the time between two consecutive abrupt changes in the RTE, by the recurrence quantification measure trapping times [11].

We consider the boundary of each peak, defined by the filling colors, as the limits of each sticky region in the Fig. 5a. From the RTE(200) time series, we compute the probability distribution of trapping times $P(t)$ for the set of trapping times $\{t_i\}_{i=1,2,\ldots,N_t}$, where $N_t$ is the total number of trapping times. Additionally, with $P(t)$, we define the cumulative distribution of trapping times as

$$Q(\tau) = \sum_{t>\tau} P(t) = \frac{N_\tau}{N_t}, \tag{16}$$

where $N_\tau$ is the number of trapping times with $t > \tau$. Figure 6a depicts the cumulative distribution of trapping times as a function of $\tau$ for each stickiness regime. The decay of trapping times obeys a power-law, with a heavy tail, which is known to be a characteristic of quasi-integrable Hamiltonian systems with stickiness [2]. On the other hand, the hyperbolic (non-sticky) region of the phase space exhibits an exponential decay of trapping times [Fig. 6b].

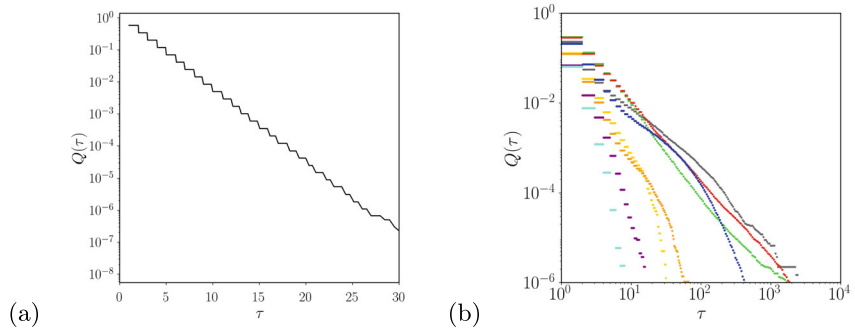


**Fig. 6** Cumulative distribution of trapping times for: **a** an orbit belonging to the hyperbolic region shown in Fig. 5d; **b** each sticky region identified in Fig. 5a with $N = 1011$ and $n = 200$ (the colors of the dots in correspond to the colors in Fig. 5a)

## 5 Conclusions

Stickiness is a typical phenomenon observed in chaotic (area-filling) orbits of non-integrable Hamiltonian systems. Chaotic orbits spend arbitrarily long times in the vicinity of periodic islands and eventually escape from them. Since the periodic islands display a complicated hierarchical structure, a sticky orbit visits the neighbourhoods of a large number of islands. It is a well-known challenge to characterize numerically sticky orbits: there have been proposed approaches based on finite-time Lyapunov exponents and finite-time rotation numbers. Recently, a novel approach using recurrence-based quantifiers has been proposed, particularly the distribution of white vertical lines in recurrence plots. From the latter, we can compute the Shannon (or recurrence time) entropy RTE.

We have applied this method to quantify dynamical properties of sticky chaotic orbits in a discrete-time mapping obtained from a plasma physics model of magnetic field lines in a Tokamak. As a general result, we find that the value of RTE is able to better characterize the nature of the orbits generated from this mapping, when compared with the largest Lyapunov exponent. Moreover, the hierarchical structure of islands around islands can be revealed by computing the finite-time RTE, whose statistical distribution displays a number of distinct peaks, each of them corresponding to the different islands visited by the sticky orbit.

We have also computed the trapping times, or the times spent by a sticky orbit in the vicinity of a given periodic island, and analysed their cumulative distribution. We discovered that the sticky behavior causes this distribution to decay as a power-law with the trapping time, whereas a hyperbolic chaotic orbit (with no stickiness) presents an exponential decay. The combination of RTE with the statistics of trapping times makes a powerful tool to characterize sticky behavior of chaotic orbits in Hamiltonian systems. Although in the present work, we have considered a specific mapping, the method and its basic features are expected to be applicable to any Hamiltonian system of physical interest.

**Acknowledgements** R. L. V. thanks the financial support from the Brazilian Federal Agencies (CNPq) under grants 403120/2021-7 and 301019/2019-3. L. C. S. thanks the financial support from the Brazilian Federal Agencies (CNPq) under grants 140713/2020-4 and of São Paulo Research Foundation (FAPESP), under Grant No. 2023/16146-6. M. R. S. acknowledges the financial support of São Paulo Research Foundation (FAPESP), under Grant No. 2023/08698-9. J. D. S. thanks the financial support from the Brazilian Federal Agencies (CNPq) under grants 311168/2020-5 and 309670/2023-3. I. L. C. thanks the financial support from the Brazilian Federal Agencies (CNPq) under grant 304616/2021-4, and the São Paulo Research Foundation (FAPESP, Brazil) under Grant No. 2018/03211-6.

## References

1. Lichtenberg, A.J., Lieberman, M.A.: Regular and Chaotic Dynamics. Springer (1992)
2. Meiss, J.D., Ott, E.: Markov tree model of transport in area-preserving maps. Physica D **20**(2–3), 387–402 (1986)
3. Latora, V.: Phys. Rev. Lett. **83**, 2104 (1999)
4. Zaslavsky, G.M.: Physica D **168–169**, 292 (2002)
5. Hazeltine, R.D., Meiss, J.D.: Plasma Confinement. Dover Books on Physics, Courier Corporation (2013)
6. Balescu, R.: Transport Processes in Plasmas. North-Holland (1988)
7. Meiss, J.D.: Thirty years of turnstiles and transport. Chaos **25**(9), 097602 (2015)
8. Meiss, J.D., Sander, E.: Birkhoff averages and the breakdown of invariant tori in volume-preserving maps. Physica D **428**, 133048 (2021)
9. Gottwald, G.A., Melbourne, I.: The 0-1 test for chaos: a review. In: Chaos Detection and Predictability, pp. 221–247 (2016)
10. Skokos, C., Antonopoulos, C., Bountis, T.C., Vrahatis, M.N.: Detecting order and chaos in Hamiltonian systems by the SALI method. J. Phys. A: Math. Gen. **37**(24), 626 (2004)
11. Marwan, N., Wessel, N., Meyerfeldt, U., Schirdewan, A., Kurths, J.: Recurrence-plot-based measures of complexity and their application to heart-rate-variability data. Phys. Rev. E **66**, 026702 (2002)
12. Marwan, N., Kurths, J.: Nonlinear analysis of bivariate data with cross recurrence plots. Phys. Lett. A **302**, 299–307 (2002)
13. Marwan, N., Romano, M.C., Thiel, M., Kurths, J.: Recurrence plots for the analysis of complex systems. Phys. Rep. **438**(5–6), 237–329 (2007)
14. Marwan, N.: A historical review of recurrence plots. Eur. Phys. J. Spec. Top. **164**(1), 3–12 (2008)
15. Slater, N.B.: Mathematical Proceedings of the Cambridge Philosophical Society, vol. 46, no. 4, pp. 525–534. Cambridge University Press (1958)
16. Slater, N.B.: Mathematical Proceedings of the Cambridge Philosophical Society, vol. 63, no. 4, pp. 1115–1123. Cambridge University Press (1967)
17. Ngamga, E.J., Senthilkumar, D.V., Prasad, A., Parmananda, P., Marwan, N., Kurths, J.: Distinguishing dynamics using recurrence-time statistics. Phys. Rev. E **85**(2), 026217 (2012)
18. Zou, Y., Thiel, M., Romano, M.C., Kurths, J.: Characterization of stickiness by means of recurrence. Chaos **17**(4), 043101 (2007)
19. Zou, Y., Pazó, D., Romano, M.C., Thiel, M., Kurths, J.: Distinguishing quasiperiodic dynamics from chaos in short-time series. Phys. Rev. E **76**, 016210 (2007)
20. Viana, R.L., Mugnaine, M., Caldas, I.L.: Hamiltonian description for magnetic field lines in fusion plasmas: a tutorial. Phys. Plasmas **30**(9), 090901 (2023)
21. Balescu, R., Vlad, M., Spineanu, F.: Tokamap: A Hamiltonian twist map for magnetic field lines in a toroidal geometry. Phys. Rev. E **58**(1), 951 (1998)

22. Szezech, J.D., Caldas, I.L., Lopes, S.R., Viana, R.L., Morrison, P.J.: Transport properties in nontwist area-preserving maps. Chaos **19**(4), 043108 (2009)
23. Little, M.A., McSharry, P.E., Roberts, S.J., Costello, D.A., Moroz, I.M.: Exploiting nonlinear recurrence and fractal scaling properties for voice disorder detection. Biomed. Eng. Online **6**, 23 (2007)
24. Baptista, M.S., Ngamga, E.J., Pinto, P.R.F., Brito, M., Kurths, J.: Kolmogorov-Sinai entropy from recurrence times. Phys. Lett. A **374**(9), 1135–1140 (2010)
25. Kraemer, K.H., Donner, R.V., Heitzig, J., Marwan, N.: Recurrence threshold selection for obtaining robust recurrence characteristics in different embedding dimensions. Chaos **28**, 085720 (2018)
26. Weissow, B., Misguich, J.H., Balescu, R.: Chaotic diffusion across a magnetic island due to a single low-frequency electrostatic wave. Plasma Phys. Controlled Fusion **33**, 763 (1991)
27. Viana, R.L.: Chaotic magnetic field lines in a Tokamak with resonant helical windings. Chaos, Solitons Fractals **11**(5), 765–778 (2000)
28. Eckmann, J.P., Kamphorst, S.O., Ruelle, D.: Recurrence plots of dynamical systems. Europhys. Lett. **4**(9), 973–977 (1987)
29. Thiel, M., Romano, M.C., Kurths, J., Meucci, R., Allaria, E., Arecchi, F.T.: Physica D **171**(3), 138–152 (2002)
30. Schinkel, S., Dimigen, O., Marwan, N.: Selection of recurrence threshold for signal detection. Euro. Phys. J. - Spec. Top. **164**(1), 45–53 (2008)
31. Eroglu, D., Peron, T.K.D., Marwan, N., Rodrigues, F.A., Costa, L.D.F., Sebek, M., Kiss, I.Z., Kurths, J.: Entropy of weighted recurrence plots. Phys. Rev. E **90**, 042919 (2014)
32. Sales, M.R., Mugnaine, M., Szezech, J.D., Jr., Viana, R.L., Caldas, I.L., Marwan, N., Kurths, J.: Stickiness and recurrence plots: an entropy-based approach. Chaos **33**, 033140 (2023)
33. Eckmann, J.P., Ruelle, D.: Ergodic theory of chaos and strange attractors. Rev. Mod. Phys. **57**(3), 617 (1985)
34. Palmero, M.S., Caldas, I.L., Sokolov, I.M.: Finite-time recurrence analysis of chaotic trajectories in Hamiltonian systems. Chaos **32**(11) (2022)
35. Souza, L.C., Sales, M.R., Mugnaine, M., Szezech, J.D., Jr., Caldas, I.L., Viana, R.L.: Chaotic escape of impurities and sticky orbits in toroidal plasmas. Phys. Rev. E **109**, 015202 (2024)
36. Szezech, J.D., Jr., Lopes, S.R., Viana, R.L.: Finite-time Lyapunov spectrum for chaotic orbits of non-integrable Hamiltonian systems. Phys. Lett. A **335**, 394–401 (2005)
37. Harle, M., Feudel, U.: Hierarchy of islands in conservative systems yields multimodal distributions of FTLEs. Chaos, Solitons & Fractals **31**(1), 130–137 (2007)